Charge Trap Formation and Passivation in Methylammonium Lead Tribromide

Xiaoyang Che, Boubacar Traoré, Claudine Katan, Hong-Hua Fang, Maria Antonietta Loi, Jacky Even, Mikaël Kepenekian

Charge Trap Formation and Passivation in Methylammonium Lead Tribromide

Xiaoyang Che,[†,‡] Boubacar Traore,[†,‡] Claudine Katan,[†] Hong-Hua Fang,[¶] Maria Antonietta Loi,[¶] Jacky Even,[*,‡] and Mikaël Kepenekian[*,†]

†*Univ Rennes, ENSCR, INSA Rennes, CNRS, ISCR (Institut des Sciences Chimiques de Rennes) - UMR 6226, F-35000 Rennes, France*

‡*Univ Rennes, INSA Rennes, CNRS, Institut FOTON - UMR 6082, F-35000 Rennes, France*

¶*Zernike Institute for Advanced Materials, University of Groningen, Groningen, Netherlands*

E-mail: jacky.even@insa-rennes.fr; mikael.kepenekian@univ-rennes1.fr

Abstract

Owing to spectacular optoelectronic properties halide perovskites hold great promises in various fields, including photovoltaics and light-emission devices. Although hybrid halide perovskites are known to be unstable when exposed durably to water and oxygen, it has been shown that humid air and oxygen can restore the photoluminescent properties of mehtylammonium lead tribromide ($MAPbBr_3$) that vanish under vacuum [Fang, H.-H. *et al. Sci. Adv.* **2016**, *2*, e1600534]. Here, thanks to density functional theory (DFT) based calculations, we propose that the quenching and revival of surface photoluminescent properties are due to the formation and passivation of surface charge traps. Moreover, we establish that bulk properties are preserved either because molecules are unlikely to penetrate the bulk, or because they do not interfere with the electronic states involved in the optical properties.

Introduction

The evolution of light to electricity conversion efficiency of hybride lead halide perovskite solar cells has witnessed an impressive improvement during the last decade,[1–3] and is now progressively becoming competitive with the commercialized silicon and thin film technologies.[4] Among their remarkable features one finds broad spectral absorption,[5–8] high absorption coefficient,[9,10] efficient charge carrier,[5,11,12] long carrier diffusion length[11,13] and, importantly, cheap and facile synthesis.[5,14–18] As a result, halide perovskites are not only promising candidates for the third generation solar cells but they also attract considerable attention of various fields. In particular, bromide perovskites show great potential in light emitting devices[19] with narrow bandwidth emission or broad white-light emission.[20–22] In addition, the multiphoton absorption of core-shell bromide perovskite colloidal nanocrystals is potentially interesting for imaging applications,[23] and its high sensitivity to γ or X-ray make them interesting photodetector materials.[24,25]

The shadow being cast over the rise of halide perovskites originates from its inherent instabilities. Those caused by chemical agents, such as water and oxygen, have been particularly studied in the recent years.[26–37] For instance, it is well known that prolonged exposure of $MAPbBr_3$ ($MA{=}CH_3NH_3^+$) to water and/or oxygen can lead to its decomposition to CH_3NH_2, $PbBr_2$, HBr and Br_2.[26] Several possible mechanisms have been suggested among which, one suggests that the presence of water on the surface of halide perovskite can potentially favors the reversible decomposition of the halide perovskite[38] while oxygen usually plays an oxidiser role and can oxidise halide to their elemental form.[38] An *ab initio* study of the $MAPbI_3$ reported by Zhang *et al.* indicates that hydroxide anion and hydroxyl radical can induce a spontanous protons transfert between these species and methylammonium cation (MA), causing the deprotonation of the latter to methylamine. They suggest this last process could be the first step of the decomposition of halide perovskite under humidity.[39] Meanwhile, since the surface properties have a strong influence on the decomposition process, efforts were made to better understand the surface morphology and the surface de-

fects of halide perovskite. *Ab initio* molecular dynamics simulations of $MAPbI_3$ have been performed on both MA-I and Pb-I terminated surfaces. They show that the MA-I terminated surfaces undergo a fast solvation process and bring out the release I atoms, while the Pb-I terminated surface exhibit higher tolerance regarding the degradation.[34] Meggiolaro and coworkers suggested possible mechanism for O_2 interaction with $MAPbI_3$ which may result in the reversible photoluminescence quantum yield enhancement.[36] In 2015, She *et al.* observed iodide vacancies located on the (001) surface of thin film of $MAPbI_3$ grown on Au (111)[40] and Ohmann *et al.* perceived the same type of vacancies for the (001) surface of a cleaved $MAPbBr_3$ crystal.[41]

The wealth of applications envisioned for bromide perovskites relies heavily on the protection of its spectacular optical properties. Interestingly, recent spectroscopy experiments carried on $MAPbBr_3$ single crystals show robust photoluminescent bulk properties and striking response of the surface under exposition of vacuum and environmental gases.[42] Indeed, the strong surface luminescence observed in normal conditions vanishes in vacuum but is recovered in the presence of humid air and oxygen. These results call for an in-depth study of the impact of these species on the electronic properties of $MAPbBr_3$. Such work should yield a better understanding of the microscopic processes at the surface of bromide perovskites.

Here, within the framework of density functional theory (DFT), we scrutinize first the effect of inclusion of water and dioxygen in $MAPbBr_3$ bulk. It is shown that this inclusion is either energetically forbidden or without significant effect on the optical properties of the material. In a second step, we focus on the (001) surface of $MAPbBr_3$ and propose surface Br vacancies to be the cause of the luminescence quenching experimentally observed because it creates a localized charge trap near the conduction bands. In addition, we inspect the passivation of the defect by water and dioxygen. In the end, $MAPbBr_3$ properties appear to be remarkably robust as long as the integrity of the perovskite structure is preserved.

Computational details

DFT calculations are performed using the SIESTA simulation package.[43] Structure relaxations are carried out with the C09 functional that takes into account van der Waals interactions.[44] Single-point calculations are performed including spin-orbit coupling (SOC) through the on-site approximation.[45] To prevent conflicts between the on-site treatment of SOC and the non-locality of C09, single-point calculations are conducted with the revPBE functional on which C09 is based.[46] Core electrons are described with norm-conserving Troullier-Martins pseudopotentials.[47] $1s^1$, $2s^2 2p^2$, $2s^2 2p^3$, $4s^2 4p^5$, and $5d^{10} 6s^2 6p^2$ are used as valence electrons for H, C, N, Br and Pb respectively. The valence wavefunctions are expanded over a double-ζ polarized basis set of finite-range numerical pseudoatomic orbitals.[48] An energy cutoff of 150 Ry for the real-space mesh is used. Structure optimisations are considered to be converged when the maximum residual force on each atom becomes smaller than 0.04 eV/Å. The Brillouin-zones are sampled with 4×4×4 and 3×3×1 Mokhorst-Pack k-grids for bulk systems and slabs, respectively. The dipoles induced in the slabs are treated with the dipole correction scheme as implemented in SIESTA.[49]

Results and discussion

Insertion of H_2O and O_2 in bulk $MAPbBr_3$. We start from the experimental structure of the low-temperature *Pnma* phase of $MAPbBr_3$.[50] The structure is fully relaxed (cell parameters and atomic positions) by means of DFT with the SIESTA simulation package (see Supporting Information, SI).[43] $MAPbBr_3$ presents a network of corner-shared $PbBr_6$ octahedra with MA cations intercalated between octahedra (Figure 1a). Cations are oriented in an anti-parallel manner leading to an anti-ferroelectric configuration with no dipole in any direction. It shows a well-known direct-gap band structure with quasi-parabolic valence and conduction bands facing at Γ (Figure 1b) in agreement with the excellent optical properties of $MAPbBr_3$. As expected from plain DFT, the computed bandgap, 1.05 eV, is largely

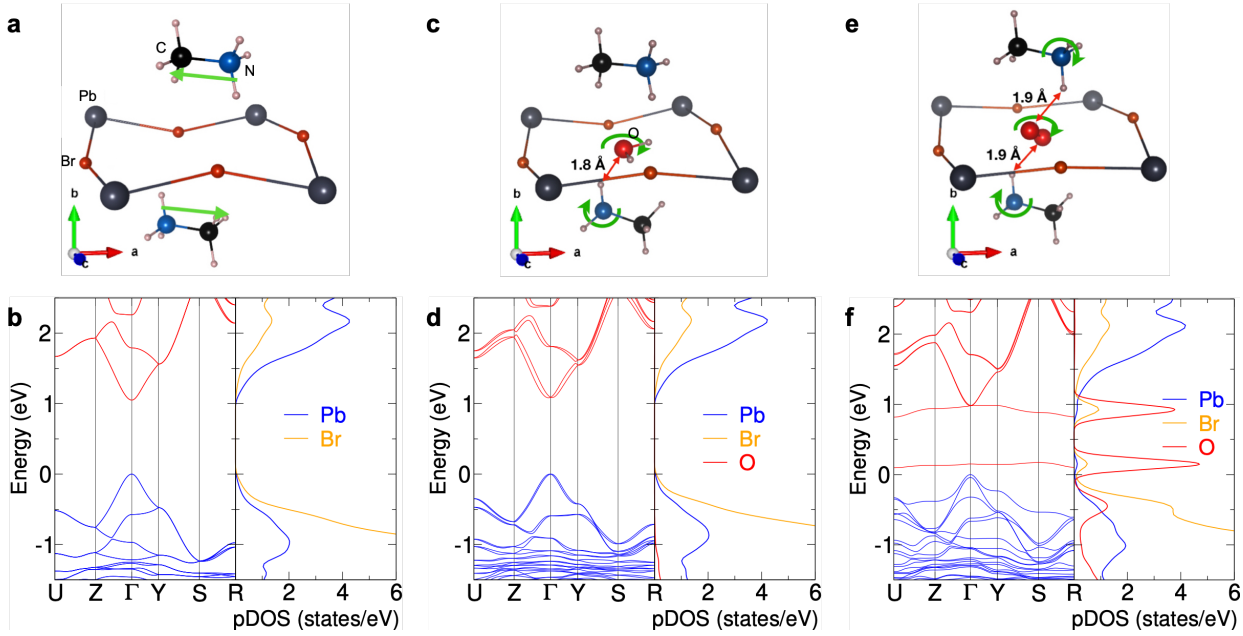

Figure 1: (a) DFT-optimized $MAPbBr_3$ low-temperature *Pnma* structure, focus on the cavity formed by the octahedra. Arrows mark the dipolar moment of MA cations. (b) Electronic band structures (left panel) and projected density of states (right panel) for the native bulk $MAPbBr_3$. The valence band maximum is taken as the energy reference. (c) Optimized structure with one H_2O molecule. Green arrows indicate the tilting of molecules. (d) Corresponding band structure. (e) Optimized structure with one O_2 molecule. (f) Corresponding band structure.

underestimated.

The structure possesses a cavity in its network of $PbBr_6$ octahedra where molecules can be inserted (Figure 1a). When one H_2O molecule is added, it occupies the cavity with H atoms pointing to Br atoms with d(H$\cdots$Br)=2.2 Å (Figure 1c). That distance compares well with the 2.3 Å of the hydrogen bond formed with free bromide ion.[51] Concomitantly, an hydrogen bond forms between the closest MA cation and H_2O (d(H$\cdots$O)=1.8 Å) causing a slight rotation of the cation. As a result, the anti-ferroelectric arrangement no longer exists and a residual dipole is expected. The inorganic framework is also affected with an elongation of Pb-Br bonds going from 2.98 to 3.05 Å leading to an overall volume expansion of 2.7%. The formation energy (Δ_f) is obtained through:

$$\Delta_f = (E_{H_2O} + E_{MAPbBr_3}) - E_{H_2O@MAPbBr_3} \quad (1)$$

where E_{H_2O}, E_{MAPbBr_3} and $E_{H_2O@MAPbBr_3}$ represent the computed total energies of the water molecule, of bulk $MAPbBr_3$, of H_2O inserted in $MAPbBr_3$, respectively. We find that the insertion of a water molecule is slightly unfavorable with $\Delta_f = 7.5$ meV per $MAPbBr_3$ unit. The resulting electronic band structure (Figure 1d) shows very little difference with the pristine structure. After insertion of H_2O, the gap opens by ca. 30 meV. This is related to the increase of the cell volume that leads to the decreasing of anti-bonding character of both valence and conduction band. Projected density of states (pDOS) show that H_2O states lie low in energy, away from the band edges, showing they will hardly influence the electronic and optical properties of $MAPbBr_3$. In addition, conduction and valence bands are split. This is due to the simultaneous presence of large SOC and the loss of centrosymmetry caused by the tilting of MA cations. This phenomena, the Rashba effect, has been well documented in halide perovskites.[52–55] Here, it is caused by our computational setup and the enforcement of periodic boundary conditions.

O_2 molecules also form hydrogen bonds with neighboring MA cations (Figure 1e) leading to a tilting of the cations and a H$\cdots$O distance of 1.9 Å. The insertion of O_2 leads to a volume expansion of 1.9% smaller than the one of H_2O. However, the formation energy is much greater with $\Delta_f = 65.0$ meV per $MAPbBr_3$ unit, rending the inclusion of O_2 unlikely. By contrast with H_2O, O_2 greatly affects the electronic structure of $MAPbBr_3$ (Figure 1f). As shown by pDOS, a set of bands due to O_2 states intercalate between the bands formed by Pb and Br states. More contributions from O_2 are found close below the valence band maximum. These states correspond to the empty anti-bonding π^* states resulting from the triplet state described for O_2, whose degeneracy is lifted by a weak interaction with the $MAPbBr_3$ network. However, the band structure of the perovskite mostly unaffected, indicating the absence of strong chemical interaction between the O_2 molecule and its host.

Therefore, the insertion of molecules, H_2O or O_2, in $MAPbBr_3$ follows two different scenarios with a common conclusion. Either the energetic cost of the insertion is low but the consequences on the optical properties are minors, or the optical properties are deeply

impacted, but the energetic cost is high and the insertion unlikely.

Surface charge traps formation and passivation. Surfaces play a determinant role in the optoelectronic properties of semiconductors since they offer numerous opportunities to form localized trap states leading, in particular, to a quenching of luminescence.[56–59] Such perturbations of optical properties have been observed on bromide perovskite crystals and nanocrystals.[42,60,61] Remarkably, good optical performances can be ensured by exposing nanocrystals to protecting species[60,61] or expose the surface to wet air or O_2 gas.[42] Here, we examine possible origin of the luminescence quenching observed at the surface of $MAPbBr_3$ under vacuum and of the recovery under selected gas.[42]

Surface phenomena are scrutinized using the (001) surface of $MAPbBr_3$ terminated by Ma-Br (Figure 3a). This termination is suggested by previous experimental and computational investigations.[40,62,63] We aim at the study of surface defects and passivation, because of the periodic boundary conditions used in our investigation, defects created in the simulation cells can interact with their periodic images. In order to limit this artifactual interaction, we have doubled the size of the cell in directions perpendicular to (001). This 2×2 supercell offers a satisfying compromise between the too limited single cell and the computationally unmanageable 3×3 supercell (Figure S1, SI). We then add a vacuum region of 85 Å along the c-axis. The resulting $MAPbBr_3$ slab contains three $PbBr_6$ octahedra along the c-axis. During the structure optimization, the lattice parameters are fixed and the bottom octahedron is kept frozen in the bulk configuration, while the rest of the structure is allowed to relax. From the pristine (001) surface (Figure 3a), we consider the removal of one {MA,Br} pair leading to a formally neutral defect (Figure 3b). The choice of halide vacancies at the surface relies on previously obtained experimental and computed results. In particular, surface halide vacancies have been characterized by scanning tunneling microscopy at the surface of $MAPbBr_3$,[41] but also at the surface of $MAPbI_3$.[40] Computational DFT-based investigations have also been conducted in the case of $MAPbBr_3$ and confirm the privileged formation of

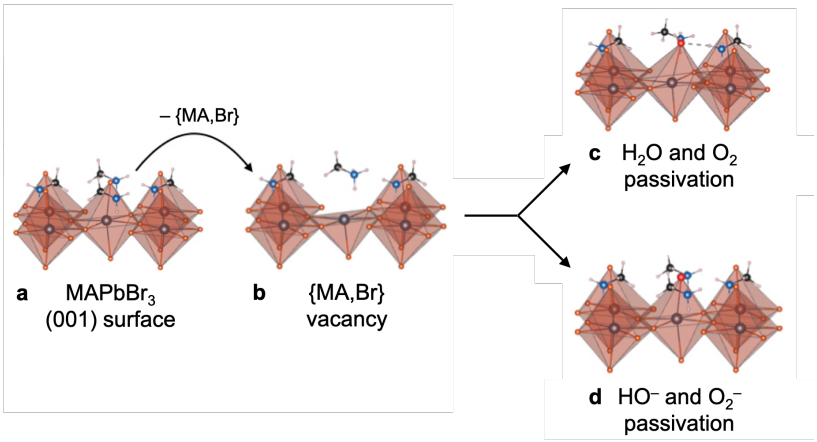

Figure 2: (a) Top layer of the pristine $MAPbBr_3$ (001) surface. (b) Same with a missing {MA,Br} pair. (c) Passivation of the defect by a neutral molecule (H_2O or O_2). (d) Passivation by an anionic molecule (HO^- or O_2^-). Pb, Br, O, N, C and H atoms are depicted in gray, orange, red, blue, black and pale pink, respectively.

neutral defects, *i.e.* {MA,Br} pairs, at the crystal surface.[64] Then, passivation (Figure 3c,d) is performed by adding either a formally neutral molecule (H_2O, O_2) or a cation/anion pair ({MA,HO}, {MA,O_2}) leading to globally neutral systems in all cases.

The (001) $MAPbBr_3$ surface maintains a direct band gap at the center of the reduced Brillouin zone (Figure 3a). Because of the confinement imposed by the use of a slab, the bandgap opens up to 1.46 eV. The partial charge densities computed at the gap edges show states delocalized on all octahedra (Figure 3b). When a defect is created at the $MAPbBr_3$ surface, under the form of a bromide vacancy, the band structure shows little variation, although the bandgap closes by 20 meV (Figure 3c). More importantly, a striking evolution occurs on the distribution of the conduction band minimum (CBM, Figure 3d). Indeed, the CBM strongly localized on the Pb atoms holding the dangling bond left by the removal of Br^-, noted Pb^*, with smaller contributions also to the Pb atoms immediately under it. Localization of states is also noticeable on the pDOS (Figure 3e). After the creation of the defect, the contribution from Pb^* shows a more localized peak at the bottom of the conduction bands, while the rest of Pb atoms show contributions identical to the one computed for the pristine surface. Therefore, the creation of a surface defect creates a localized charge trap within the band gap that is likely to promote nonradiative recombination of charges

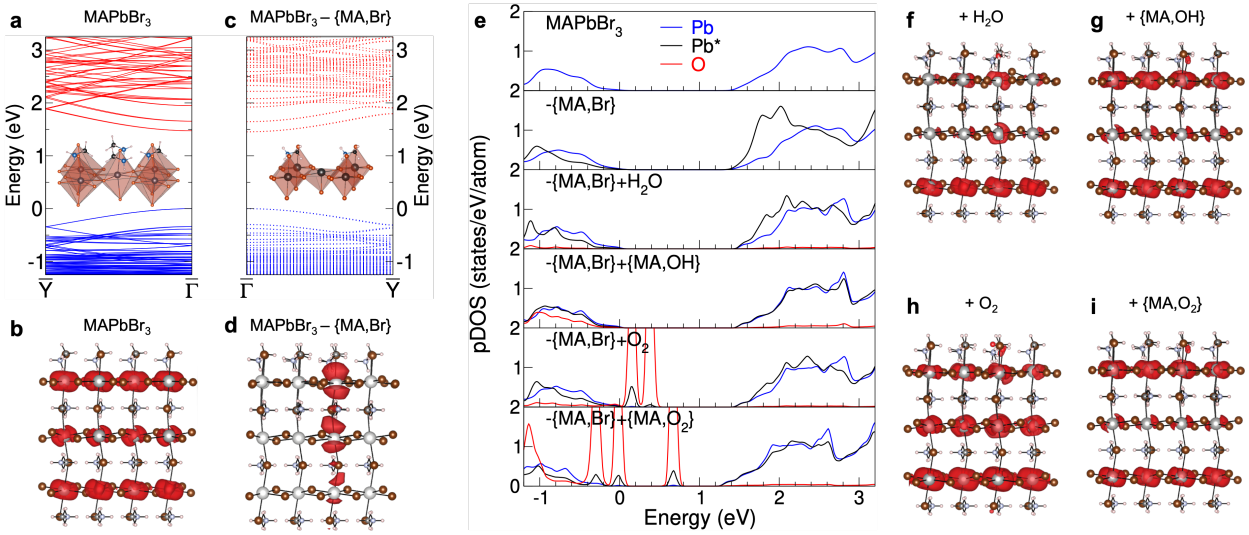

Figure 3: (a) Band structure of $MAPbBr_3$ (001) surface. (b) Corresponding partial charge density computed at the conduction band minimum (CBM). (c) Band structure of $MAPbBr_3$ (001) presenting a {MA,Br} vacancy. (d) Corresponding partial charge density computed at the CBM. (e) Projected density of states (pDOS) computed for the pristine $MAPbBr_3$ (001) surface, the {MA,Br} vacancy, its passivation by H_2O, {MA,OH}, O_2 and {MA,O_2}. DOS are projected on O (red lines), on the Pb atom holding the dangling bond (noted Pb*, black lines), on other Pb atoms (blue lines). Partial charge densities of the $MAPbBr_3$ (001) surface passivated by (f) H_2O, (g) {MA,OH}, (h) O_2 and (i) {MA,O_2}.

over efficient emission. This is in agreement with the vanishing luminescence experimentally observed on $MAPbBr_3$ monocrystals when subject to vacuum.[42]

In the set of experiments carried out by Fang *et al.*, luminescence is recovered after exposition under humid air and dioxygen.[42] Here, we survey the potential passivation of the {MA,Br} vacancy by small molecules found in environmental gases. We begin with H_2O. The molecule places itself on top of the sub-coordinated lead atom with the oxygen substituting the Br atom. As shown by the pDOS and the charge density (Figure 3e,f), the new environment of Pb* contributes to partially restore the delocalized nature of the CBM found in the emitting pristine $MAPbBr_3$ surface. The passivation remains however incomplete with a still marked localized CBM. On the other hand, if one consider the hydroxide anion HO^- as passivated agent, the contribution from Pb* becomes alike those of other Pb atoms (Figure 3e) and the CBM recovers its delocalized nature (Figure 3g).

Similar behaviors are observed in the case of O_2 and the superoxide O_2^-. Indeed, O_2

shows only partial passivation of the Pb^* dangling bond (Figure 3e,h), while O_2^- exhibits complete passivation with both pDOS and charge densities pointing to a fully recovered CBM (Figure 3i). Notably, both species are accompanied by the apparition of supplementary mid-gap states due to the oxygen species.

In the end, H_2O and O_2 act as L-type ligands coordinating Pb^*, while HO^- and O_2^- behave as X-type ligands. The former fail to repair the perturbation caused by surface vacancies, while the latter can fulfill Pb^* dangling bonds and cancel the charge trap likely to extinguish the strong surface luminescence of $MAPbBr_3$.

Conclusions

Halide perovskites present interesting optoelectronic properties including bright luminescence. We have examined the robustness of this feature with respect to water and oxygen in the case of $MAPbBr_3$. Firstly, we have shown that the insertion of H_2O or O_2 molecules inside a crystal was either unlikely (O_2) or with no consequence on the optical properties of the material (H_2O), as long as its overall structure is preserved. Naturally, the material remains sensitive to water and oxygen and prolonged exposition can eventually lead to the decomposition of the material.[26] Then, we have focused on surface effects and in particular the occurence of bromide defects that would leave a lead dangling bond. Our investigation establishes that such a vacancy generates a localized charge trap at the bottom of the conduction band that is likely to quench the radiative recombination. Focusing on environmental gases, we found that hydroxide and superoxide anions successfully passivate the lead atom and restore a fully delocalized charge, thus cancelling the charge trap. These observations are in excellent agreement with the spectroscopic results obtained on monocrystals of $MAPbBr_3$.[42] This work delivers essential ingredients to preserve optical properties of halide perovskite crystals and nanocrystals that have strong potential as active materials in light emitting devices.

Acknowledgement

The work at Institut des Sciences Chimiques de Rennes and Institut FOTON was supported by Agence National pour la Recherche (SuperSansPlomb and TRANSHYPERO projects). This work was granted access to the HPC resources of [TGCC/CINES/IDRIS] under the allocation 2017-A0010907682 made by GENCI. H.H. Fang and M.A. Loi acknowledge the financial support of the European Research Council (ERC Starting Grant Hy-SPOD No. 306983).

Supporting Information Available

Additional information on surface simulation cells.

References

(1) Kojima, A.; Teshima, K.; Shirai, Y.; Miyasaka, T. Organometal Halide Perovskites as Visible-Light Sensitizers for Photovoltaic Cells. *J. Am. Chem. Soc.* **2009**, *131*, 6050–6051.

(2) Yang, W. S.; Park, B.-W.; Jung, E. H.; Jeon, N. J.; Kim, Y. C.; Lee, D. U.; Shin, S. S.; Seo, J.; Kim, E. K.; Noh, J. H. et al. Iodide management in formamidinium-lead-halide–based perovskite layers for efficient solar cells. *Science* **2017**, *356*, 1376–1379.

(3) https://www.nrel.gov/pv/assets/images/efficiency-chart.png.

(4) Yoshikawa, K.; Kawasaki, H.; Yoshida, W.; Irie, T.; Konishi, K.; Nakano, K.; Uto, T.; Adachi, D.; Kanematsu, M.; Uzu, H. et al. Silicon heterojunction solar cell with interdigitated back contacts for a photoconversion efficiency over 26%. *Nat. Energy* **2017**, *2*, 17032.

(5) Lee, M. M.; Teuscher, J.; Miyasaka, T.; Murakami, T. N.; Snaith, H. J. Efficient Hybrid Solar Cells Based on Meso-Superstructured Organometal Halide Perovskite. *Science* **2012**, *338*, 643–647.

(6) Kazim, S.; Nazeeruddin, M. K.; Grätzel, M.; Ahmad, S. Perovskite as light harvester: A game changer in photovoltaics. *Angew. Chem. Int. Ed.* **2014**, *53*, 2812–2824.

(7) Stoumpos, C. C.; Kanatzidis, M. G. The Renaissance of Halide Perovskites and Their Evolution as Emerging Semiconductors. *Acc. Chem. Res.* **2015**, *48*, 2791–2802.

(8) Stranks, S. D.; Nayak, P. K.; Zhang, W.; Stergiopoulos, T.; Snaith, H. J. Formation of thin films of organic-inorganic perovskites for high-efficiency solar cells. *Angew. Chem. Int. Ed.* **2015**, *54*, 3240–3248.

(9) Green, M. A.; Ho-Baillie, A.; Snaith, H. J. The emergence of perovskite solar cells. *Nature Photon.* **2014**, *8*, 506–514.

(10) Brenner, T. M.; Egger, D. A.; Kronik, L.; Hodes, G.; Cahen, D. Hybrid organic - Inorganic perovskites: Low-cost semiconductors with intriguing charge-transport properties. *Nat. Rev. Mater.* **2016**, *1*, 15007.

(11) Xing, G.; Mathews, N.; Sun, S.; Lim, S. S.; Lam, Y. M.; Grätzel, M.; Mhaisalkar, S.; Sum, T. C. Long-Range Balanced Electron- and Hole-Transport Lengths in Organic-Inorganic $CH_3NH_3PbI_3$. *Science* **2013**, *342*, 344–347.

(12) Miyata, A.; Mitioglu, A.; Plochocka, P.; Portugall, O.; Wang, J. T. W.; Stranks, S. D.; Snaith, H. J.; Nicholas, R. J. Direct measurement of the exciton binding energy and effective masses for charge carriers in organic-inorganic tri-halide perovskites. *Nat. Phys.* **2015**, *11*, 582–587.

(13) Stranks, S. D.; Eperon, G. E.; Grancini, G.; Menelaou, C.; Alcocer, M. J. P.; Leijtens, T.; Herz, L. M.; Petrozza, A.; Snaith, H. J. Electron-hole diffusion lengths exceeding 1 micrometer in an organometal trihalide perovskite absorber. *Science* **2013**, *342*, 341–344.

(14) Snaith, H. J. Perovskites: The emergence of a new era for low-cost, high-efficiency solar cells. *J. Phys. Chem. Lett.* **2013**, *4*, 3623–3630.

(15) Kim, H. S.; Lee, C. R.; Im, J. H.; Lee, K. B.; Moehl, T.; Marchioro, A.; Moon, S. J.; Humphry-Baker, R.; Yum, J. H.; Moser, J. E. et al. Lead iodide perovskite sensitized all-solid-state submicron thin film mesoscopic solar cell with efficiency exceeding 9%. *Sci. Rep.* **2012**, *2*, 591.

(16) Liu, M.; Johnston, M. B.; Snaith, H. J. Efficient planar heterojunction perovskite solar cells by vapour deposition. *Nature* **2013**, *501*, 395–398.

(17) Grätzel, M. The light and shade of perovskite solar cells. *Nat. Mater.* **2014**, *13*, 838–842.

(18) Jeon, N. J.; Noh, J. H.; Yang, W. S.; Kim, Y. C.; Ryu, S.; Seo, J.; Seok, S. I. Compositional engineering of perovskite materials for high-performance solar cells. *Nature* **2015**, *517*, 476–480.

(19) Akkerman, Q. A.; Rainò, G.; Kovalenko, M. V.; Manna, L. Genesis, challenges and opportunities for colloidal lead halide perovskite nanocrystals. *Nat. Mater.* **2018**, *17*, 394–405.

(20) Dohner, E. R.; Hoke, E. T.; Karunadasa, H. I. Self-assembly of broadband white-light emitters. *J. Am. Chem. Soc.* **2014**, *136*, 1718–1721.

(21) Dohner, E. R.; Jaffe, A.; Bradshaw, L. R.; Karunadasa, H. I. Intrinsic white-light emission from layered hybrid perovskites. *J. Am. Chem. Soc.* **2014**, *136*, 13154–13157.

(22) Mao, L.; Guo, P.; Kepenekian, M.; Hadar, I.; Katan, C.; Even, J.; Schaller, R. D.; Stoumpos, C. C.; Kanatzidis, M. G. Structural Diversity in White-Light-Emitting Hybrid Lead Bromide Perovskites. *J. Am. Chem. Soc.* **2018**, *140*, 13078–13088.

(23) Chen, W.; Bhaumik, S.; Veldhuis, S. A.; Xing, G.; Xu, Q.; Grätzel, M.; Mhaisalkar, S.; Mathews, N.; Sum, T. C. Giant five-photon absorption from multidimensional core-shell halide perovskite colloidal nanocrystals. *Nat. Commun.* **2017**, *8*, 15198.

(24) Mao, L.; Wu, Y.; Stoumpos, C. C.; Wasielewski, M. R.; Kanatzidis, M. G. White-Light Emission and Structural Distortion in New Corrugated Two-Dimensional Lead Bromide Perovskites. *J. Am. Chem. Soc.* **2017**, *139*, 5210–5215.

(25) Wei, H.; Fang, Y.; Mulligan, P.; Chuirazzi, W.; Fang, H. H.; Wang, C.; Ecker, B. R.; Gao, Y.; Loi, M. A.; Cao, L. et al. Sensitive X-ray detectors made of methylammonium lead tribromide perovskite single crystals. *Nat. Photonics* **2016**, *10*, 333–339.

(26) Wang, Z.; Shi, Z.; Li, T.; Chen, Y.; Huang, W. Stability of Perovskite Solar Cells: A Prospective on the Substitution of the A Cation and X Anion. *Angew. Chem. Int. Ed.* **2017**, *56*, 1190–1212.

(27) Niu, G.; Li, W.; Meng, F.; Wang, L.; Dong, H.; Qiu, Y. Study on the stability of $CH_3NH_3PbI_3$ films and the effect of post-modification by aluminum oxide in all-solid-state hybrid solar cells. *J. Mater. Chem. A* **2014**, *2*, 705–710.

(28) Clegg, C.; Hill, I. G. Systematic study on the impact of water on the performance and stability of perovskite solar cells. *RSC Adv.* **2016**, *6*, 52448–52458.

(29) Aristidou, N.; Eames, C.; Sanchez-Molina, I.; Bu, X.; Kosco, J.; Saiful Islam, M.; Haque, S. A. Fast oxygen diffusion and iodide defects mediate oxygen-induced degradation of perovskite solar cells. *Nat. Commun.* **2017**, *8*, 15218.

(30) Müller, C.; Glaser, T.; Plogmeyer, M.; Sendner, M.; Döring, S.; Bakulin, A. A.; Brzuska, C.; Scheer, R.; Pshenichnikov, M. S.; Kowalsky, W. et al. Water Infiltration in Methylammonium Lead Iodide Perovskite: Fast and Inconspicuous. *Chem. Mater.* **2015**, *27*, 7835–7841.

(31) Zhu, Z.; Hadjiev, V. G.; Rong, Y.; Guo, R.; Cao, B.; Tang, Z.; Qin, F.; Li, Y.; Wang, Y.; Hao, F. et al. Interaction of Organic Cation with Water Molecule in Perovskite $MAPbI_3$: From Dynamic Orientational Disorder to Hydrogen Bonding. *Chem. Mater.* **2016**, *28*, 7385–7393.

(32) Mosconi, E.; Meggiolaro, D.; Snaith, H. J.; Stranks, S. D.; De Angelis, F. Light-induced annihilation of Frenkel defects in organo-lead halide perovskites. *Energy Environ. Sci.* **2016**, *9*, 3180–3187.

(33) Xu, R. P.; Li, Y. Q.; Jin, T. Y.; Liu, Y. Q.; Bao, Q. Y.; O'Carroll, C.; Tang, J. X. In Situ Observation of Light Illumination-Induced Degradation in Organometal Mixed-Halide Perovskite Films. *ACS Appl. Mater. Interfaces* **2018**, *10*, 6737–6746.

(34) Mosconi, E.; Azpiroz, J. M.; De Angelis, F. Ab Initio Molecular Dynamics Simulations of Methylammonium Lead Iodide Perovskite Degradation by Water. *Chem. Mater.* **2015**, *27*, 4885–4892.

(35) He, Y.; Wang, S. Q.; Xue, X. X.; Zhang, L.; Chen, K.; Zhou, W. X.; Feng, Y. Ab initio study of the moisture stability of lead iodine perovskites. *J. Phys. : Condens. Matter.* **2018**, *30*.

(36) Meggiolaro, D.; Mosconi, E.; De Angelis, F. Mechanism of Reversible Trap Passivation by Molecular Oxygen in Lead-Halide Perovskites. *ACS Energy Lett.* **2017**, *2*, 2794–2798.

(37) Zhang, L.; Sit, P. H. Ab initio study of the dynamics of electron trapping and detrapping processes in the CH3NH3PbI3 perovskite. *J. Mater. Chem. A* **2019**, *7*, 2135–2147.

(38) Ahmad, S.; Kanaujia, P. K.; Niu, W.; Baumberg, J. J.; Vijaya Prakash, G. In situ intercalation dynamics in inorganic-organic layered perovskite thin films. *ACS Appl. Mater. Interfaces* **2014**, *6*, 10238–10247.

(39) Zhang, L.; Sit, P. H.-L. Ab Initio Study of Interaction of Water, Hydroxyl Radicals, and Hydroxide Ions with $CH_3NH_3PbI_3$ and $CH_3NH_3PbBr_3$ Surfaces. *J. Phys. Chem. C* **2015**, *119*, 22370–22378.

(40) She, L.; Liu, M.; Zhong, D. Atomic Structures of $CH_3NH_3PbI_3$ (001) Surfaces. *ACS Nano* **2015**, *10*, 1126–1131.

(41) Ohmann, R.; Ono, L. K.; Kim, H.-S.; Lin, H.; Lee, M. V.; Li, Y.; Park, N.-G.; Qi, Y. Real-Space Imaging of the Atomic Structure of Organic-Inorganic Perovskite. *J. Am. Chem. Soc.* **2015**, *137*, 16049–16054.

(42) Fang, H.-H.; Adjokatse, S.; Wei, H.; Yang, J.; Blake, G. R.; Huang, J.; Even, J.; Loi, M. A. Ultrahigh sensitivity of methylammonium lead tribromide perovskite single crystals to environmental gases. *Sci. Adv.* **2016**, *2*, e1600534.

(43) Soler, M.; Artacho, E.; Gale, J. D.; Garc, A.; Junquera, J.; Ordejón, P.; Daniel, S. The SIESTA Method for Ab initio Order-N materials Simulation. *J. Phys. : Condens. Matter.* **2002**, *14*, 2745–2779.

(44) Cooper, V. R. Van der Waals density functional: An appropriate exchange functional. *Phys. Rev. B* **2009**, *81*, 161104.

(45) Fernández-Seivane, L.; Oliveira, M. A.; Sanvito, S.; Ferrer, J. On-site approximation for spin-orbit coupling in linear combination of atomic orbitals density functional methods. *J. Phys.: Condens. Matter* **2006**, *18*, 7999–8013.

(46) Zhang, Y.; Yang, W. Comment on "Generalized Gradient Approximation Made Simple". *Phys. Rev. Lett.* **1998**, *80*, 890.

(47) Troullier, N.; Martins, J. L. Efficient pseudopotentials for plane-wave calculations. *Phys. Rev. B* **1991**, *43*, 1993–2006.

(48) Artacho, D., E.and Sánchez-Portal; Ordejón, P.; García, A.; Soler, J. M. Linear-Scaling ab-initio Calculations for Large and Complex Systems. *phys. stat. sol. (b)* **1999**, *215*, 809–817.

(49) Bengtsson, L. Dipole correction for surface supercell calculations. *Phys. Rev. B* **1999**, *59*, 12301–12304.

(50) Swainson, I. P.; Hammond, R.; Soullière, C.; Knop, O.; Massa, W. Phase transitions in the perovskite methylammonium lead bromide, $CH_3ND_3PbBr_3$. *J. Solid. State Chem.* **2003**, *176*, 97–104.

(51) Emsley, J. In *The elements*; Polytechnica,, Ed.; Oxford University Press, 1998.

(52) Kepenekian, M.; Robles, R.; Katan, C.; Sapori, D.; Pedesseau, L.; Even, J. Rashba and Dresselhaus Effects in Hybrid Organic Inorganic Perovskites: From Basics to Devices. *ACS Nano* **2015**, *9*, 11557–11567.

(53) Brivio, F.; Butler, K. T.; Walsh, A.; van Schilfgaarde, M. Relativistic quasiparticle self-consistent electronic structure of hybrid halide perovskite photovoltaic absorbers. *Phys. Rev. B* **2014**, *89*, 155204.

(54) Mosconi, E.; Umari, P.; De Angelis, F. Electronic and optical properties of MAPbX3 perovskites (X = I, Br, Cl): a unified DFT and GW theoretical analysis. *Phys. Chem. Chem. Phys.* **2016**, *18*, 27158–27164.

(55) Kepenekian, M.; Even, J. Rashba and Dresselhaus Couplings in Halide Perovskites: Accomplishments and Opportunities for Spintronics and Spin-Orbitronics. *J. Phys. Chem. Lett.* **2017**, *8*, 3362–3370.

(56) Jones, M.; Nedeljkovic, J.; Ellingson, R. J.; Nozik, A. J.; Rumbles, G. Photoenhancement of Luminescence in Colloidal CdSe Quantum Dot Solutions. *J. Phys. Chem. B* **2003**, *107*, 11346–11352.

(57) Liu, Y.-H.; Wayman, V. L.; Gibbons, P. C.; Loomis, R. A.; Buhro, W. E. Origin of High Photoluminescence Efficiencies in CdSe Quantum Belts. *Nano Lett.* **2010**, *10*, 352–357.

(58) Mooney, J.; Krause, M. M.; Saari, J. I.; Kambhampati, P. A Microscopic Picture of Surface Charge Trapping in Semiconductor Nanocrystals. *J. Chem. Phys.* **2013**, *138*, 204705.

(59) Demortière, A.; Schaller, R. D.; Li, T.; Chattopadhyay, S.; Krylova, G.; Shibata, T.; dos Santos Claro, P. C.; Rowland, C. E.; Miller, J. T.; Cook, R. et al. In Situ Optical and Structural Studies on Photoluminesence Quenching in CdSe/CdS/Au Heterostructures. *J. Am. Chem. Soc.* **2014**, *136*, 2342–2350.

(60) Nenon, D. P.; Pressler, K.; Kang, J.; Koscher, B. A.; Olshansky, J. H.; Osowiecki, W. T.; Koc, M. A.; Wang, L.-W.; Alivisatos, A. P. Design Principles for Trap-Free $CsPbX_3$ Nanocrystals: Enumerating and Eliminating Surface Halide Vacancies with Softer Lewis Bases. *J. Am. Chem. Soc.* **2018**, *140*, 17760–17772.

(61) Bodnarchuk, M. I.; Boehme, S. C.; ten Brinck, S.; Bernasconi, C.; Shynkarenko, Y.; Krieg, F.; Widmer, R.; Aeschlimann, B.; Günther, D.; Kovalenko, M. V. et al. Rationalizing and Controlling the Surface Structure and Electronic Passivation of Cesium Lead Halide Nanocrystals. *ACS Energy Lett.* **2019**, *4*, 63–74.

(62) Komesu, T.; Huang, X.; Paudel, T. R.; Losovyj, Y. B.; Zhang, X.; Schwier, E. F.; Kojima, Y.; Zheng, M.; Iwasawa, H.; Shimada, K. et al. Surface Electronic Structure of Hybrid Organo Lead Bromide Perovskite Single Crystals. *J. Phys. Chem. C* **2016**, *120*, 21710–21715.

(63) Che, X.; Traore, B.; Katan, C.; Kepenekian, M.; Even, J. Does Rashba splitting in $CH_3NH_3PbBr_3$ arise from 2×2 surface reconstruction? *Phys. Chem. Chem. Phys.* **2018**, *20*, 9638–9643.

(64) Liu, Y.; Palotas, K.; Yuan, X.; Hou, T.; Lin, H.; Li, Y.; Lee, S.-T. Atomistic Origins of Surface Defects in CH 3 NH 3 PbBr 3 Perovskite and Their Electronic Structures. *ACS Nano* **2017**, *11*, 2060–2065.

Graphical TOC Entry

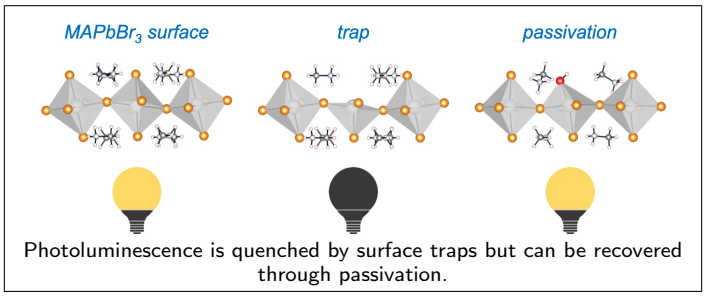

Charge Trap Formation and Passivation in Methylammonium Lead Tribromide Supporting Information

Xiaoyang Che,[†,‡] Claudine Katan,[†] Hong-Hua Fang,[¶] Maria Antonietta Loi,[¶] Jacky Even,[*,‡] and Mikaël Kepenekian[*,†]

†*Univ Rennes, ENSCR, INSA Rennes, CNRS, ISCR (Institut des Sciences Chimiques de Rennes) - UMR 6226, F-35000 Rennes, France*

‡*Univ Rennes, INSA Rennes, CNRS, Institut FOTON - UMR 6082, F-35000 Rennes, France*

¶*Zernike Institute for Advanced Materials, University of Groningen, Groningen, Netherlands*

E-mail: jacky.even@insa-rennes.fr; mikael.kepenekian@univ-rennes1.fr

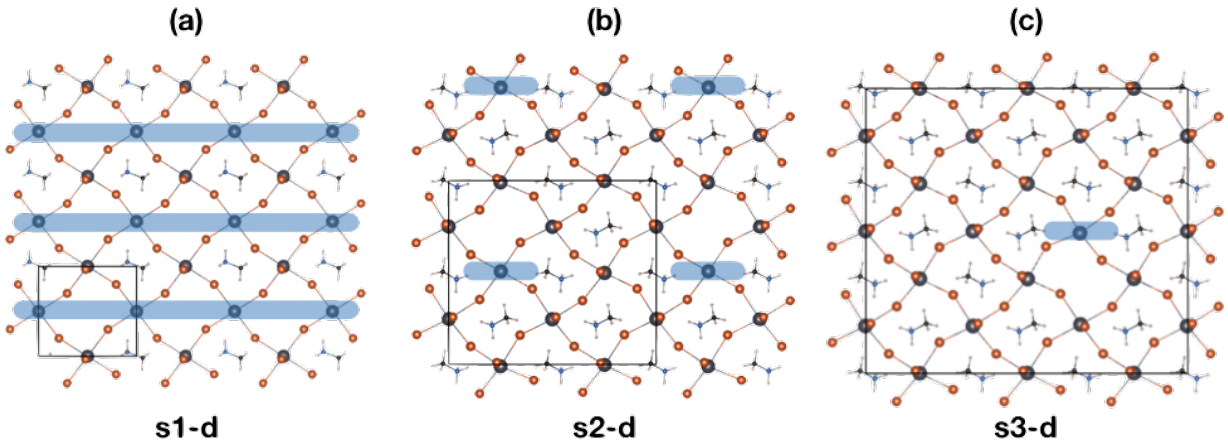

Figure S1: Top views of the (001) surface of $MAPbBr_3$ deprived of one MA and one Br per simulation cell. Blue rectangles highlight the missing atoms. For clarity, only the top layer is displayed. (a) The single *Pnma* cell is used. The removal of one {MA,Br} couple per unit leaved a line of defects because of periodic boundary conditions. (b) Same with a 2×2 supercell. Defects are now separated. (c) Same with a 3×3 supercell. Defects are further apart, but the computational cost becomes unmanageable.